Design and testing of a contra-rotating tidal current turbine

J A Clarke, G Connor, A D Grant and C M Johnstone
Energy Systems Research Unit,
University of Strathclyde
Glasgow, Scotland, UK.
esru@strath.ac.uk

Abstract

A contra-rotating marine current turbine has a number of attractive features: near-zero reactive torque on the support structure, near-zero swirl in the wake, and high relative inter-rotor rotational speeds. Modified blade element modelling theory has been used to design and predict the characteristics of such a turbine, and a model turbine and test rig have been constructed. Tests in a towing tank demonstrated the feasibility of the concept. Power coefficients were very high for such a small model and in excellent agreement with predictions, confirming the accuracy of the computational modelling procedures.

High-frequency blade loading data were obtained in the course of the experiments. These show the anticipated dynamic components for a contra-rotating machine. Flow visualisation of the wake verified the lack of swirl behind the turbine. A larger machine is presently under construction for sea trials.

Keywords: - marine currents, turbine, contra-rotating, model tests.

Notation

a axial velocity reduction factor

a' tangential velocity factor

C_D blade drag coefficient

C_L blade lift coefficient

C_N normal thrust coefficient

C_P turbine power coefficient

C_T tangential force coefficient

r radius at blade element

V_∞ free stream velocity

W fluid velocity relative to blade

λ blade tip speed ratio

ρ fluid density

σ rotor solidity

φ flow angle (see Figs 1 and 2)

Ω rotor angular velocity

1. Introduction

Recent policy statements in the UK **[1], [2]** have set ambitious targets for renewable energy exploitation. Marine currents have been identified as an important potential contributor because the energy yield and time of occurrence may be predicted in advance.

The fluid dynamics of marine current turbines are similar to those of wind turbines. However, there are important differences in the character of the flow: it is restrained by boundaries above and below, and to some extent at the sides. Levels of velocity shear and turbulence (affecting both velocity and direction) may also differ; in the absence of comprehensive, reliable data one can only speculate. A major advantage for marine turbines is that maximum current velocities have definite, rather than statistical limits.

In most cases so far, marine current turbine prototypes closely follow conventional wind turbine practice, with 2 or 3-bladed horizontal-axis rotors **[3].** But the technology is far from mature, and it may be beneficial to adopt other ideas. Some of these were first postulated for wind energy but not fully developed. An example is the contra-rotating turbine, using co-

axial rotors in close proximity, which in wind energy conversion most recently appeared as the Trimblemill **[4].** For wind power it may be difficult to justify the added complexity of the rotor configuration, but the potential advantages of the layout are particularly significant in a marine context: -

- near-zero reaction torque on the supporting structure, simplifying structural design and mooring arrangements;
- near-zero swirl in the wake of the turbine, reducing scouring of the sea bed downstream;
- high relative rotational speeds, simplifying (or even eliminating) the geared drive to the generator;
- increased power output.

After preliminary feasibility studies **[5]** it was decided to proceed with a small prototype for testing and evaluation.

2. Turbine design

Simple blade element theory when applied to a conventional, single-rotor turbine equates forces on the blade and on the fluid stream, through the equations

$$dF = 4\pi r\rho V_\infty{}^2\, a(1-a)dr = \pi\rho\sigma W\left[C_L\,\Omega r(1+a') + C_D V_\infty(1-a)\right]r.dr$$

for the axial, streamwise component and

$$dS = 4\pi r^2\rho V_\infty(1-a)a'\Omega.dr = \rho W\sigma\left[C_L V_\infty(1-a) - C_D\,\Omega\, r(1+a')\right]r.dr$$

for the tangential component.

These equations are solved by an iterative process to produce converged values of the flow parameters *a* and *a*', after which the velocity vectors shown in Figure 1 may be evaluated. Performance predictions for the complete rotor are obtained from a summation over all blade elements, making an appropriate allowance for blade tip losses.

In predicting the performance of a contra-rotating pair of rotors, certain assumptions must be made. In this study, it was assumed that the rotors are in close proximity, and function as a single actuator disc as far as blade element theory is concerned. Secondly, it was assumed that the swirl imparted to the flow by the upstream rotor is completely removed by the rotor downstream, i.e. there is zero reaction torque transferred to the structure which supports the rotor pair. The procedure adopted was to prescribe a geometry for the upstream rotor, obtain converged solutions for *a* and *a*', and use these to specify an appropriate geometry for the downstream rotor.

To obtain a closed solution to the momentum equation for the upstream rotor, a further assumption is required. It is clear that the equation above for *dF* is no longer correct: the upstream rotor will only experience a fraction of the total retarding force on the fluid stream, and it is necessary to specify this fraction for the equation to be solved. In practice a wide range of conditions may occur, and these would need to be investigated. But also in practice, a rotor would be designed for optimum performance in certain specified flow conditions.

For these initial, exploratory calculations, a "symmetrical" case was used, where the rotors run at the same tip speed ratio and it was assumed that each experiences the same axial thrust loading, equal of course to one half of that experienced by the fluid stream. Therefore

$\lambda_1 = \lambda_2$, $dF_1 = dF_2$, and $dS_1 = dS_2$, where subscripts 1 and 2 refer to upstream and downstream rotors respectively.

Extending this to each blade element, the equation for *dF* is modified to

$$dF = 2\pi r \rho V_\infty^{\,2}\, a(1-a)dr = \pi \rho \sigma W \left[C_L\, \Omega r (1+a') + C_D V_\infty (1-a)\right] r.dr$$

for the upstream rotor. The equations were then solved to give values of *a* and *a*'. For the rotor as a whole, parameters such as axial thrust, torque and power output may be computed at this stage.

For the downstream rotor, the velocity and force vector diagrams (Figure 2) are similar, but not identical, to those upstream. The flow angle φ is obtained from

$$\tan \phi = \frac{V_\infty (1-a)}{\Omega r}$$

so φ is known if a has been determined. The momentum equations reduce to

$$\frac{\sigma C_N}{2} = \frac{a}{1-a} \sin^2 \varphi \quad \text{and} \quad \frac{\sigma C_T}{4} = a' \sin \varphi . \cos \varphi ,$$

where $C_N = C_L \cos\varphi + C_D \sin\varphi$ is the axial or normal thrust coefficient, and

$C_T = C_L \sin\varphi - C_D \cos\varphi$ is the tangential force coefficient.

They may be combined to eliminate σ, giving $\frac{C_T}{C_N} \tan\varphi = \frac{2a'(1-a)}{a}$.

This equation is solved by iteration: values of the blade pitch angle β are presented until a solution is found. Solidity σ is then calculated, and the blade chord length determined.

A solution for a small turbine is illustrated in Figure 3. The aerofoil section used for both rotors was the NREL S814. Overall diameter was 0.82 m, with 3 blades upstream and 4 downstream. The tip speed ratio for each rotor was 3. Distributions of blade chord length and pitch angle (beta) show similar but not identical trends for the two rotors. Some numerical instability was observed in calculations near the tip for the second rotor, apparently due to the effects of tip losses. In this region, values of chord and pitch extrapolated from trends further inboard were used in the production specifications. With these adjustments, the design was adopted for the model turbine to be used in tank tests. The predicted power coefficient for the complete assembly at the specified tip speed ratio was 0.3846.

3. Performance predictions for the model turbine

A second computational code, again based on blade element theory, was then used to predict the performance of this model turbine for a range of operating conditions. Inputs to the code

consisted of blade geometries for the two rotors, the stream velocity and the tip speed ratio for each rotor. Blade chord and pitch distributions predicted by the original design code were extracted as polynomial equations, to be used as data input for these subsequent calculations (and later for CNC machining of the blades themselves). As before, it was assumed that the torques on the two rotors should be equal, giving zero net reaction torque. However, axial thrust loadings need not be equal when running off-design.

At first, an attempt was made to replicate the design condition of $\lambda_1 = \lambda_2 = 3$. As with the previous code, it was necessary to specify the ratio of axial thrust loadings for the rotors at the outset. The code would then predict the torque and thrust for each rotor. For the design condition, of course the values for each rotor should be the same.

For off-design conditions (say $\lambda_1 = 4$), the procedure was to specify values of λ_2 and axial thrust ratio, and iterate until a solution was found in which the torques were equal and the axial thrust ratio equalled the specified value. So a series of operating points were found for selected values of λ_1.

Predictions for the design condition provided a searching test of the original design code, and the results obtained were encouraging. For zero net reaction torque at $\lambda_1 = 3$, the precise conditions required were $\lambda_2 = 2.875$, with an axial thrust distribution of 51% / 49% for the upstream and downstream rotors respectively. This contrasts with the 50% / 50% axial thrust distribution and $\lambda_2 = 3$ specified in the original design. Given that blade chord and pitch data were not identical to the outputs from the design code (having been smoothed somewhat for ease of manufacture) some small discrepancies would be expected. Full C_P / λ characteristics were then determined for the turbine, C_P being the overall power coefficient and $\lambda = \lambda_1 + \lambda_2$.

The performance prediction code also permitted investigation of the effect of changing blade pitch angle, a facility which was available on the test model simulated here. A comparison of C_P / λ characteristics is shown in Figure 4, showing the effect of increasing pitch angles (on

both rotors) by 2° and 4°. It is apparent that the nominal blade angle settings for this design do not maximise the value of C_P, and a small increase in pitch angle is desirable. Then, peak values well above 0.4 are attainable. Even at the nominal blade angle setting, maximum C_P is not reached at the design tip speed ratio of 6, but somewhat higher.

4. Test model

A model turbine was then constructed for tank testing. Blades were cut from T6082 aluminium alloy on a CNC milling machine, using patterns derived from the computational design process. Split hubs clamped the blade roots while allowing infinite variation of pitch angle. The two co-axial stainless steel rotor shafts ran underwater in plain polymer bearings without lubrication. A CAD schematic of the submerged drive train is shown in Figure 5.

It was considered impractical to fit a submerged generator to such a small model, so loading was applied by mechanical friction. To meet the condition of zero net torque, the same brake load had to be applied to each rotor; however, it was important that the rotors were free to turn at different speeds. A differential gearbox was constructed to meet these criteria and frictional load was applied by a small disc brake, hydraulically actuated. Brake and gearbox were located above the water surface, drive from the rotors travelling via bevel gear sets and vertical semi-rigid drive-shafts. The co-axial rotor shafts were housed in a cylindrical shroud, attached to a vertical beam, which in turn was clamped to the carriage of the towing tank. The complete assembly, raised out of the water for inspection, is shown in Figure 6. When testing, the submerged section of the beam was fitted with a streamlined fairing to reduce pressure build-up and drag; Figure 7 gives a clearer view of the rotor assembly with the fairing in place.

The overall diameter of each rotor was 0.82 m. Axial spacing between the rotors was adjustable, from 45mm (the practical minimum) to 100mm.

5. Instrumentation

The following quantities were to be measured: carriage speed, rotor shaft speeds, main beam bending moment and brake arm bending moment. Also, the in-plane and normal bending moments were measured on one blade from each rotor. Data sampling and processing were performed by LabView software.

Transfer of strain gauge data from the two contra-rotating rotors posed some problems. Initially each rotor hub contained a compact data storage device in the form of a WAV format recorder; however timing synchronisation for fast dynamic analysis was insufficiently reliable. The final solution employed the multiplexing of high frequency electrical signals from the 4 strain gauge channels (normal and edgewise on each rotor) via slip-rings to a single LabView input channel. Data de-multiplexing was carried out in software to reproduce the strain-gauge data sampled at 1300 Hz, equating to a rotor angular strain-gauge resolution smaller than 1^{o}. Regulated full-bridge gauging amplification circuitry ensured consistent results with environmental and power variations.

6. Test procedure and results

6.1 Procedure

The tests were carried out at a single depth of immersion and a fixed carriage speed of 0.8 m/s, which was found to be sufficient for stable running. The Reynolds number based on rotor diameter was therefore about 6.5×10^{5}. Runs were made with increasing brake loads until one or both rotors stalled. A number of rotor axial spacings and blade pitch angles were investigated.

6.2 Power Coefficient

The mechanical drive train of the test turbine imposed a significant resistive torque even in the absence of any applied friction at the disc brake. Blade root bending moments were therefore used to calculate shaft torque and hence power output. Experimental values of power coefficient were plotted against tip speed ratio as superimposed points in Figure 4. The maximum turbine power output in all tests at 0.8 m/s towing speed was directly measured as 127 W, corresponding to a peak C_p of 0.39.

6.3 Dynamic Effects

Time series recordings from the strain gauge bridges are presented in Figure 8. These indicate blade root bending moments in the plane of rotation, and normal to this plane, for one blade in each rotor. In the captions, R1 refers to the upstream 3-bladed rotor, R2 to the 4-bladed rotor downstream. A period of 2.75 s is displayed, covering more than 2 complete revolutions for each rotor. This particular record was obtained with the turbine running close to its maximum power coefficient, with a tip speed ratio of 7.25.

6.4 Turbine wake

Turbulence and swirl were qualitatively investigated by use of wool streamers attached behind the turbine within the wake. Underwater video footage of the same area behind the turbine allowed examination of the wool streamers during test-runs; additionally small particles in the flow were clearly visible on the video sequences.

7. Discussion

7.1 Power coefficient

Only two sets of results have so far been fully analysed. At nominal blade pitch angle, the agreement with predictions of power coefficient is remarkably good. For pitch angles 2 degrees above nominal, excellent agreement is again seen at high tip speed ratios, but

significant discrepancies are apparent elsewhere. This series of tests was carried out with a larger inter-rotor spacing, and the downstream rotor tended to stall under heavy loads. The minimum stable tip speed ratio was limited to 7, and performance at slightly higher ratios seemed to be adversely affected. Also of course, wide spacing between rotors departs from the "single actuator disc" assumption implicit in the blade element theory of the computational model. Examination of other test data series should clarify the issue.

7.2 Blade loads and dynamic effects

From both predictions and experimental observations, it is clear that blade bending loads are very large for marine current turbines. In a real operating environment (as distinct from a towing tank), dynamic loading from velocity shear, rotor misalignment and water-borne turbulence must be considered. For rotors near the surface, waves may add a significant cyclic load **[6]**. Finally, blade/strut interaction will create a once-per-revolution perturbation.

In a contra-rotating turbine, further cyclic loads from blade/blade interaction would be expected. For the turbine tested, with 3 and 4 blades, disturbances might occur at frequencies of $4(P_1 + P_2)$ for the upstream rotor and $3(P_1 + P_2)$ for the downstream one, where P_1 and P_2 are the rotational frequencies of the upstream and downstream rotors respectively.

Detailed analysis of experimental blade bending moment data has not been completed, but some general conclusions may be drawn from Figure 8. Normal (stream-wise) loads for rotor 1 are reasonably steady, as expected. Also as expected, data for rotor 2 show more variation, with perturbations in some places coming at a frequency consistent with blade/blade interaction.

Edge moments (in the plane of rotation) for rotor 1 are again fairly steady, with a small-amplitude 1*P* ripple caused by gravity. Signals for rotor 2 show much larger excursions, and are still under investigation. The lengthy, gear-driven power take-off system of the test

model may be a factor here. The large number of "spikes" in the edge moments for both rotors may have the same cause.

7.3 Turbine wake

Only a qualitative study of the wake has been made at this stage. Wool streamers attached to the hub exhibited very little turbulence and tended to lie in line with the main direction of flow even in close proximity to the downstream rotor. This was reinforced by observing the transit through the turbine of particles suspended in the water where again, little swirl was observable.

8. Conclusions

Tests in a towing tank have demonstrated that a contra-rotating turbine with near-zero reactive torque on the support structure, near-zero swirl in the wake, and high relative inter-rotor rotational speeds can operate successfully.

Power coefficients were very high for such a small model. The excellent agreement with predicted values has established confidence in the novel aspects of the computational models used in the design procedure.

High-frequency blade loading data were obtained in the course of the experiments. These show the anticipated dynamic components for a contra-rotating machine. Flow visualisation of wake flows verified the lack of swirl behind the turbine.

9. Further Work

Data analysis from the tank tests is not yet complete. Further studies will include a systematic investigation of the effects of inter-rotor spacing, and a comprehensive analysis of dynamic blade loads.

Model studies into mooring options are in progress, after which a larger (3 m diameter) version of the turbine will be deployed in sea trials.

Acknowledgement

The authors wish to thank Scottish Enterprise, for funding through their "Proof of Concept" programme the work which is described in this paper.

References

[1] UK Government Department of Trade and Industry, 2003, Our energy future – creating a low carbon economy, DTI, London, UK, URN 03/658.

[2] Scottish Executive, 2003, Securing a renewable future: Scotland's renewable energy, Scottish Executive, Edinburgh, UK, ISBN 0-7559-0766-3.

[3] Myers I and Bahaj A S, 2004, Basic operational parameters of a horizontal axis marine current turbine, *Proceedings of World Renewable Energy Congress*, Denver, USA.

[4] Stobart A F, 1983, Wind energy: some notes on its collection, storage and application, *Energy World*, pp 4-6.

[5] Clarke J A, Grant A D and Johnstone C M, 2003, Development of a novel rotor-generator for tidal current energy conversion, Proceedings of the *IoM Parsons Turbine Conference*, Dublin.

[6] Barltrop N, Grant A D, Varyani K S, Pham X P, 2005, Wave-current interactions in marine current turbines, Proceedings of the *6th European Wave and Tidal Energy Conference*, Glasgow.

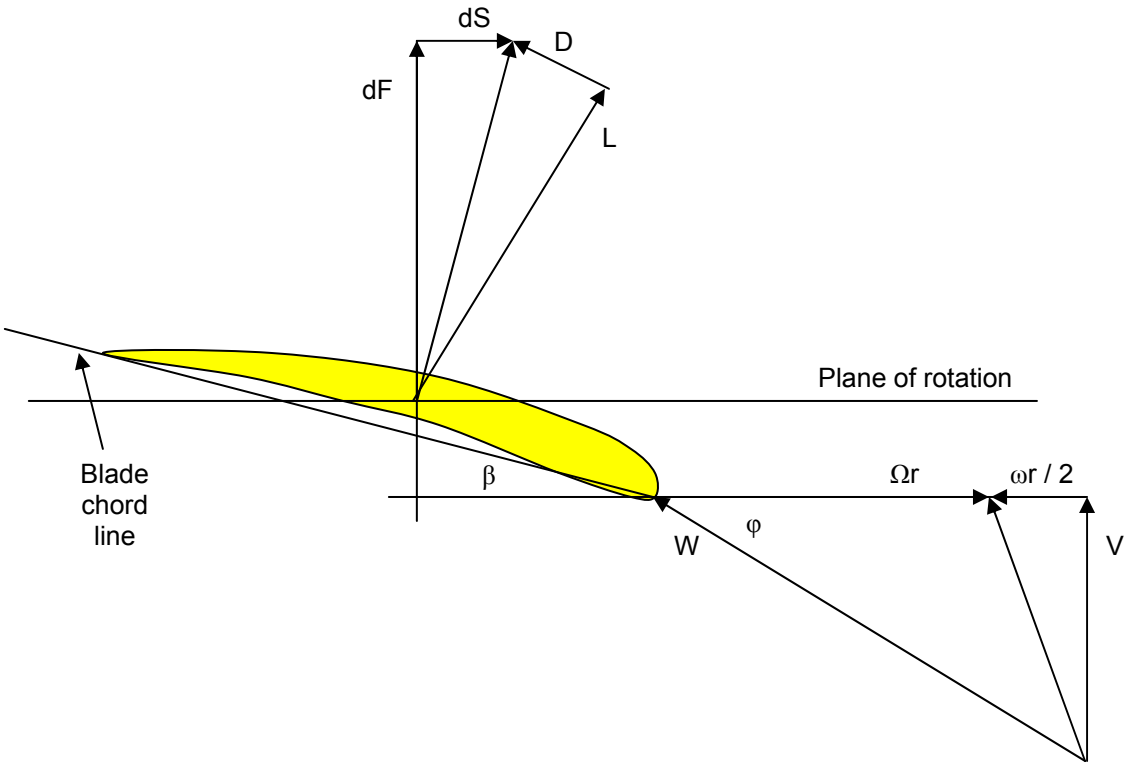

Figure 1: Vector diagram for up-stream rotor.

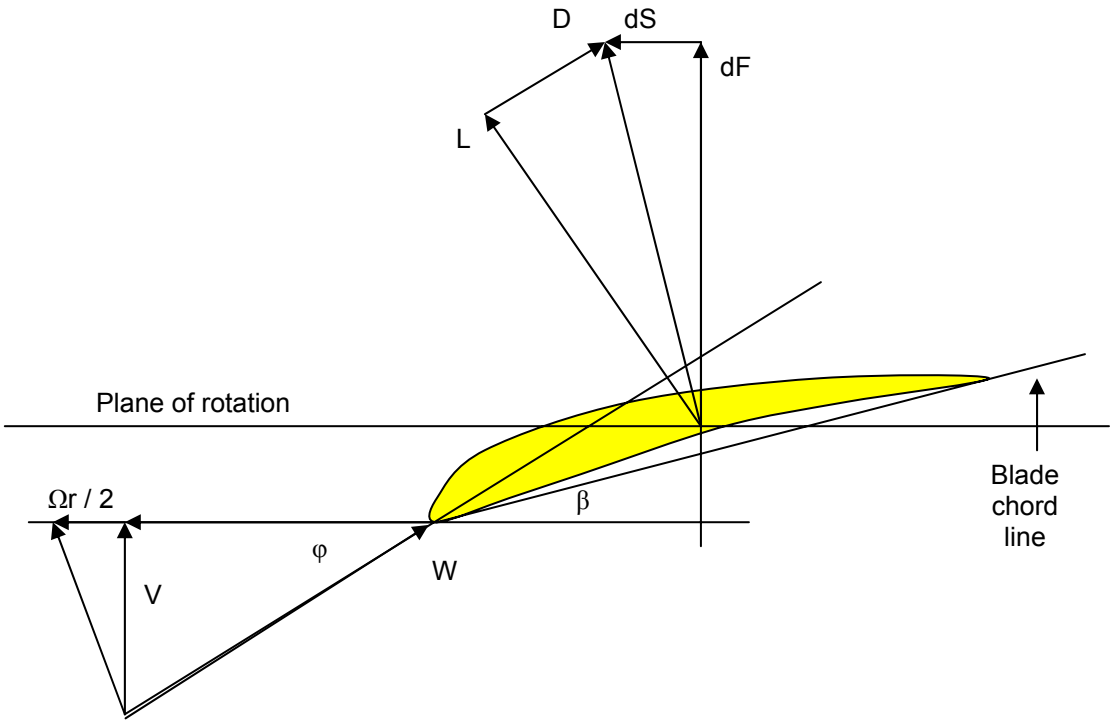

Figure 2: Vector diagram for down-stream rotor.

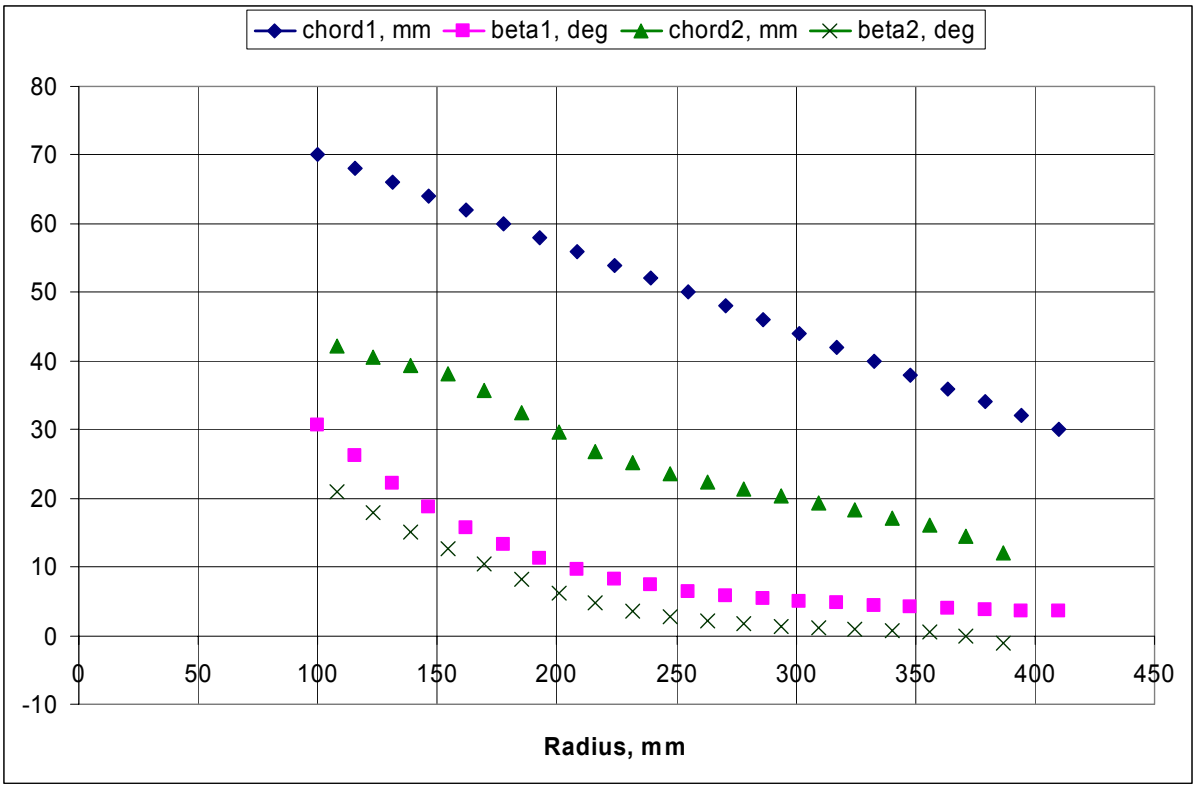

Figure 3: Design blade chord and pitch distributions for the contra-rotating turbine model.

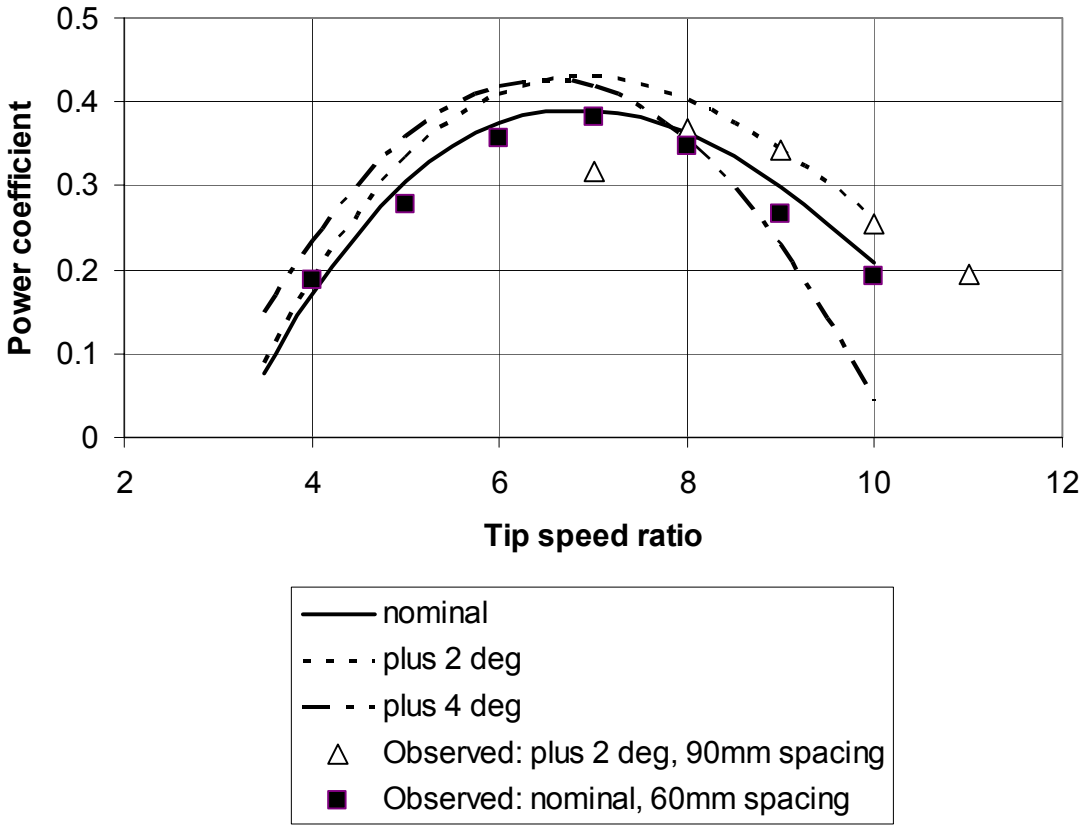

Figure 4: Effects of blade pitch angle change on rotor performance.

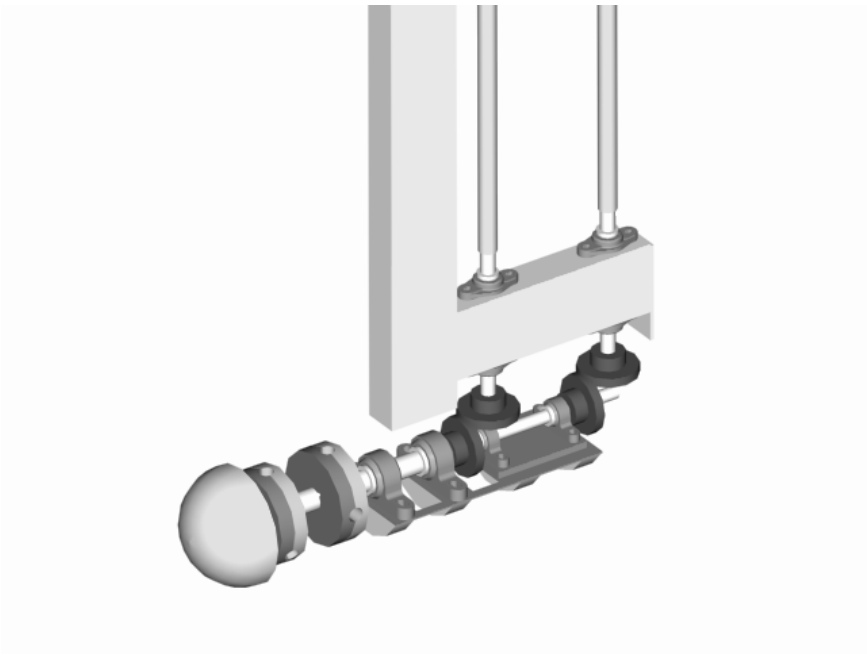

Figure 5: CAD rendering showing drive train detail.

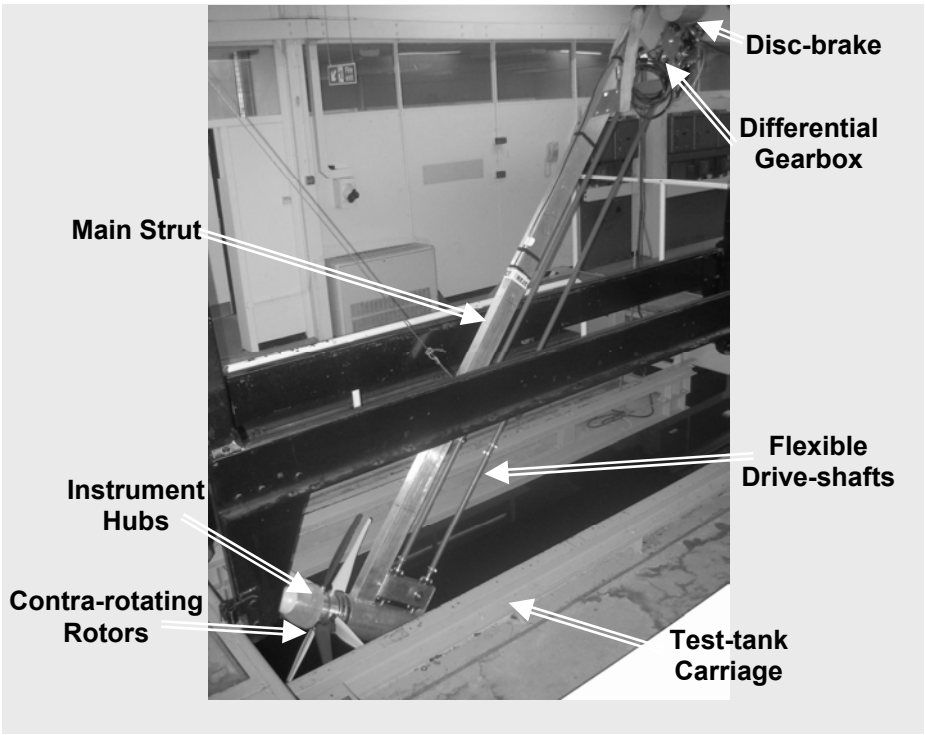

Figure 6: The test-rig raised out of the tank and on the carriage.

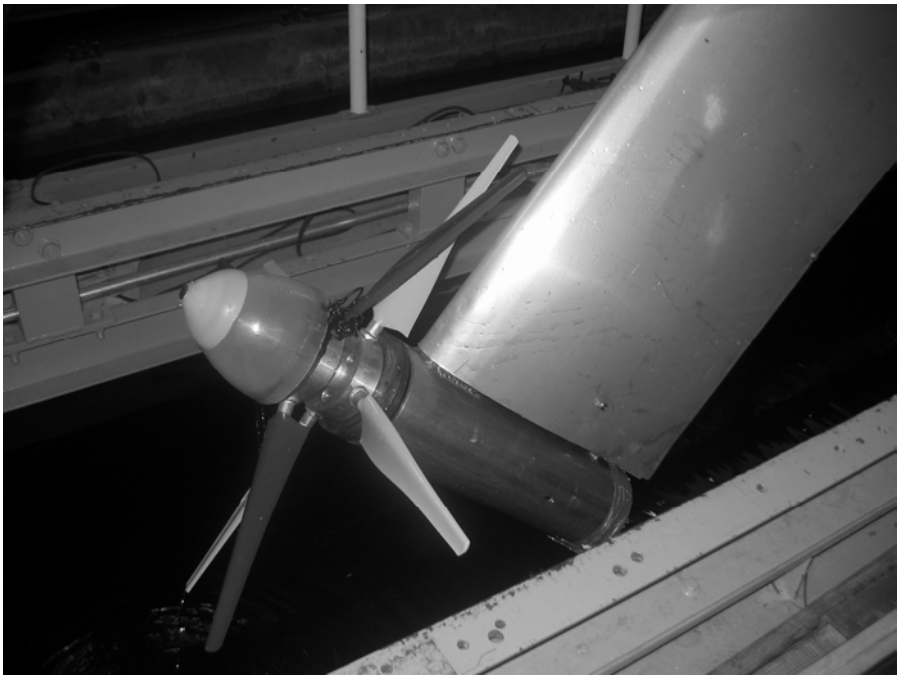

Figure 7: Contra-rotating turbine and fairing on the test rig.

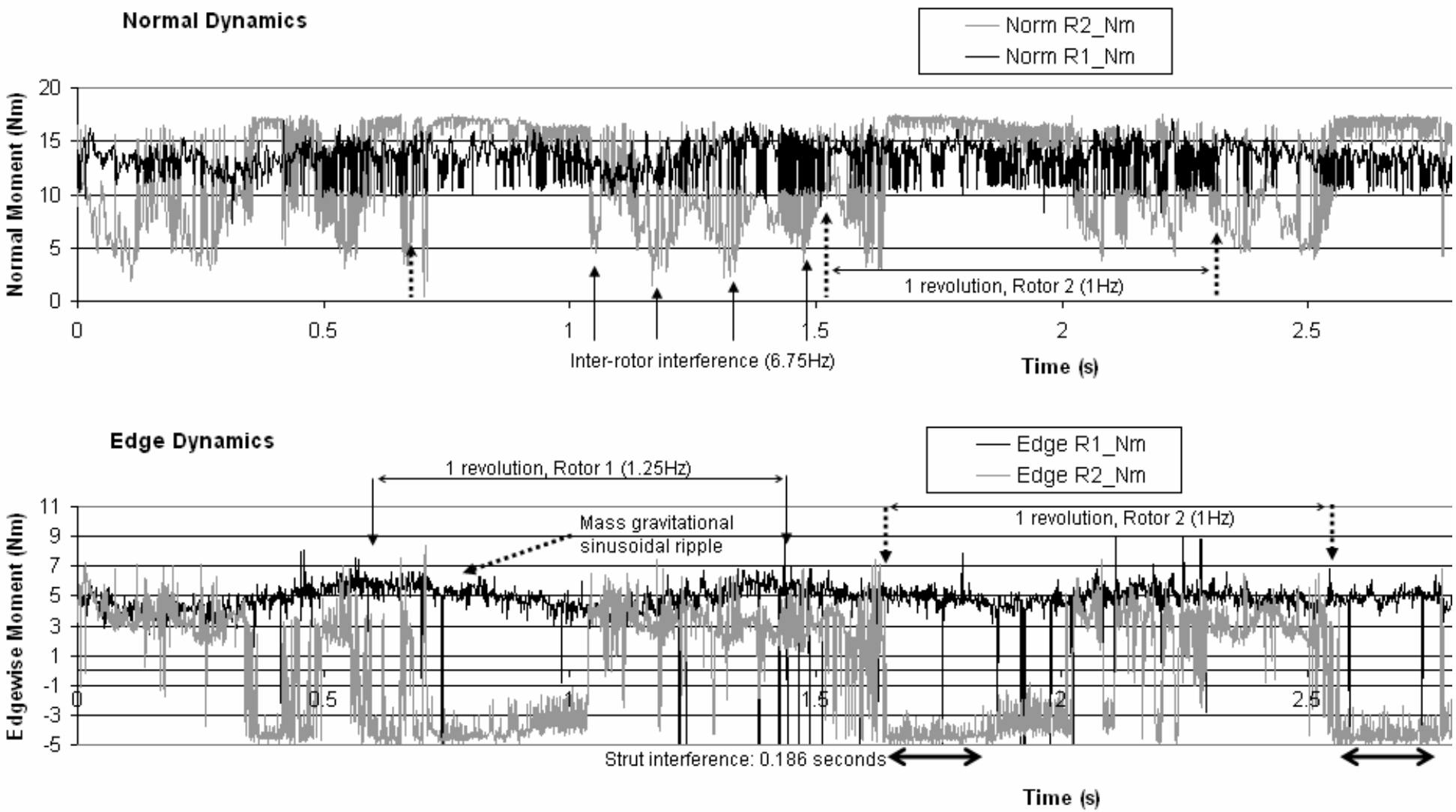

Figure 8: Blade root bending moments in two planes